Ⓔ

Modeling Strong Ground Motion in the Wellington Metropolitan Area, New Zealand

by Rafael Benites and Kim B. Olsen

Abstract   The Wellington Metropolitan Area, New Zealand, about 35 km by 10 km, is crossed by the southernmost segment of the Wellington fault, striking roughly in the northeast–southwest direction. Numerical modeling of M 6.7 earthquakes due to ruptures on this fault, intended to characterize the 3D effects of the region's main geological features on the ground motion, are performed by using a finite-differences scheme with staggered grid, for frequencies up to 1.5 Hz. We consider the part of the Wellington fault that crosses the Wellington Metropolitan Region as an almost vertical strike-slip fault, 30 km long, and with slip distribution history taken from the slip history of the 1992 M 7.3 Landers, California, earthquake. The 3D stratigraphy of the region has been built by integrating all available geological and geophysical data. Results of the modeling show several dominant features. When the fault ruptures from south to north, resonance occurs within a small area close to the harbor, where the depth of the basin is largest. This resonance produces a train of seismic waves traveling northward with dominant frequency of about 0.5 Hz. As the rupture propagates into the harbor, the radiated wavefield focuses on the Lower Hutt Valley, to the north, due to the presence of a ridge that rises up from the bottom of the harbor to emerge as Somes Island. This effect considerably enhances the incident seismic energy in the valley, particularly the horizontal motions. Further focusing occurs due to the triangular shape of the Lower Hutt Valley, whose alluvial deposits exhibit large impedance contrasts with the surrounding bedrock. The combined focusing effects produce amplification factors in the valley of about 5 between 0.5 Hz and 0.7 Hz. In Wellington City the amplification factors are between 0.5 (deamplification) and 2, except for an area on reclaimed land in the harbor, which shows an amplification factor as large as 9. After the rupture has stopped, higher frequency waves, between 1 and 1.2 Hz, appear trapped (reverberating) in the harbor for the remaining duration of the seismograms, up to 60 sec. On the other hand, when the rupture is from north to south, none of the focusing effects occur. Only the long-lasting reverberations in the harbor seem a characteristic of the wave propagation common to both rupture directions. Nevertheless, the amplification factors in this north-to-south scenario are about the same as for the south-to-north rupture.

Online material: Movies of Wellington Fault rupture scenarios.

Introduction

Our study considers the cities of Wellington and Lower Hutt as the Wellington Metropolitan area, on the North Island of New Zealand. In plan view this is a rectangular area of about 10 km by 35 km, with areas of modern urban development, business districts, and industrial infrastructure. Figure 1 shows the model location and the Wellington fault, enclosed by the white line rectangle, in the southern tip of the North Island. This region is crossed by the southernmost segment of the Wellington fault, of about 75-km length, called the Wellington–Hutt Valley Segment (Langridge *et al.*, 2005; Berryman, 1990).

There have been no major earthquakes on this fault segment known to European settlers (since about 1840), but paleoseismic studies reveal that this is an active fault, with an almost vertical fault plane extending to about 20-km depth, of strike-slip mechanism, and with a return period
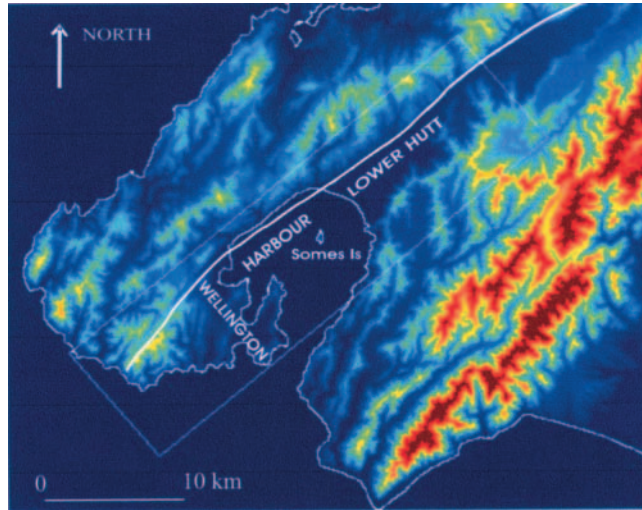
Figure 1. The Wellington region model location. The rectangle depicts the plan view outline of our 3D velocity model, showing the Wellington Fault trace (thick white line), and the coastline. Variation in color denotes topography; blue is sea level.

between 420 and 780 years for a magnitude between *M* 7.0 and 7.8. It has ruptured at least twice in the past 1000 years, and it ruptured most recently between 350 and 500 years ago (Van Dissen *et al.*, 1992). There is also paleoseismic evidence that the average surface slip is between 3.4 and 4.7 m in large past events, corresponding to magnitudes within *M* 7.0 and 7.8 (Berryman, 1990). In general, the most likely rupture scenario of this fault in terms of spatial initiation point, direction of rupture, and average slip over the whole fault is not known. In the absence of historical earthquakes, our main purpose is to characterize the strong ground motion in the Wellington metropolitan area by numerically simulating the seismic wave propagation for large earthquakes due to several hypothetical rupture scenarios of the Wellington fault. The scenarios reported in this article involve ruptures of 35 km of the Wellington–Hutt Valley Segment depicted in Figure 1, corresponding to a magnitudes *M* 6.7. Scenarios involving the rupture of the 75-km segment, corresponding to magnitude about *M* 7.5, will be the subject of a separate study.

The ground motion in parts of the Wellington region was studied previously using observed weak motion not generated by events on the Wellington fault. A thorough study of the Lower Hutt area was carried out by Taber and Smith (1992), using temporary deployments of seismic stations at a total of 24 sites, with frequency coverage between 0.5 and 12 Hz. They found that amplification increased with thickness of the sediments toward the south of the valley, yielding factors up to 14 between 1 and 3 Hz, with respect to a station on rock. They also found amplification at lower frequencies, down to 0.5 Hz. Dellow *et al.* (1992) assessed the ground shaking by correlation with the type of soils. They also gave

a detailed description of the geological materials in the region.

A comprehensive study of microzone effects in the Hutt Valley using strong-motion instruments was performed by Sritharan and McVerry (1992), who analyzed accelerograms from weak to moderate ground motion in the frequency range from 0.5 to about 8 Hz (nine earthquakes of magnitudes between 4.9 and 7 corresponding to epicentral distances 70 km and 240 km, respectively) which provided accelerations of up to 0.1g. Their results show that amplification (computed by Fourier spectral ratio of the ground motion on sediments with respect to a reference station on rock) varies systematically with the thickness of the sediments across the Lower Hutt Valley. For example, for frequencies over 2 Hz, the maximum amplification factor of nearly 12 occurs at a site with sediment deposits only 20-m thick, while for frequencies less than 1 Hz the maximum amplification factor of about 5 occurs at a site with sediments 300-m thick. This latter peak amplification factor occurs at 0.6 Hz, and it also appears in the 5% damped response spectral ratios of other sites on the sediments with respect to rock, although not as the maximum value. This peak at 0.6 Hz is particularly relevant to our study.

Adams (2000) modeled *SH* waves in 2D cross sections of the Lower Hutt Valley perpendicular to the fault, emphasizing the generation of surface waves at the fault bounded edge of the basin, also called basin edge effects. Further modeling of the *SV* component was desirable, since the component perpendicular to the fault (upon fault rupture) can be larger than the component parallel to the fault strike. Adams *et al.* (2003) analyzed the weak motion recorded by 12 stations aligned perpendicularly to the fault in the Lower Hutt area and found high variability of the ground motion at closely (50 m) spaced stations, peak amplifications between 2 and 2.5 Hz, and Love waves with fundamental Airy phase frequency also between 2 and 2.5 Hz. They attributed these characteristics to basin edge effects.

At this stage, our goal is to incorporate in the modeling some important geological features of the region, such as the fault (down to 8.6 km), the 3D basin bedrock topography, and the 3D irregular soil layers deposited over the bedrock, and compute the wave propagation for frequencies up to 1.5 Hz. The soil layers exhibit, in turn, velocity and density gradients with depth. We believe that the low-frequency effects of those geological features on the ground motion can be well characterized by the range of wavelengths involved in our calculations, the smallest being 200 m in the softest soil of *S*-wave velocity of 300 m/sec. This implies that the 12 km by 5 km Lower Hutt Valley has dimensions of 60 × 25 wavelengths. We have not included the free-surface topography of the region, nor the softer soils (*S*-wave velocity less than 300 m/sec). This is mainly due to computer limitations, which we expect to overcome in later studies. The flat, free surface in our case has been chosen with respect to a datum level 40 m above sea level. The 3D crustal model is described in Table 1.

Table 1
3D Crustal Model Specification

Description	S-Wave Velocity (m/sec)	Density (kg/m³)
Soft Last Glacial sediments	300	2200
Stiff Last Interglacial sediments	330	2275
Poorly consolidated Waimea sediments	460	2359
Poorly consolidated Kororo Interglacial sediments	475	2365
Stiff Waimaunga Glacial sediments	610	2415
Stiff Brunswick Interglacial sediments	615	2417
Stiff weathered undifferentiated sediments	700	2421
Lithified, fractured basement rock (graywacke)	1500	2744

The Wellington Fault and the Metropolitan Region's Crustal Model

We consider the Wellington Fault as a vertical strike-slip fault 35 km long and 8.6 km wide, that is, of area of about 301 km², or 70% of the equivalent fault area that ruptured during the 1994 M 6.7 Northridge, California, earthquake. Such a length is just under one half of the total length of the Wellington–Hutt Valley fault segment, which is expected to break in the event of a characteristic earthquake of M 7 +. Both the 35-km length and the 8.6-km width of the fault are chosen here to comply with the computer limitations imposed by the maximum physical size of the model. In addition, this section of the fault has been divided into 13 segments in order to accommodate the corresponding curved surface trace (Berryman, 1990).

The fault is embedded in a 3D stratigraphic model of the Wellington metropolitan area, generated from the integration of all available geological and geophysical (borehole, bathymetry, gravity, and seismic) data, down to about 800-m depth. This determines three irregular layers of sediments over bedrock (graywacke) in the Lower Hutt Valley and the harbor areas, with S-wave velocity varying between 300 m/sec and 500 m/sec in the top layer, 475 m/sec and 700 m/sec in the middle layer, and 700 m/sec and 1500 m/sec in the bottom layer. The S-wave velocity of the bedrock is 1500 m/sec, and the depth of the basin–bedrock interface varies between 0 m (free surface) and 580 m. The bedrock interface extends down to 900-m depth, where we incorporate the standard Wellington 1D crustal model routinely used for hypocenter determination (Robinson, 1986) to represent the medium below, down to 10-km depth. From this model we have taken V_p = 5400 m/sec, V_s = 3200 m/sec, and ρ = 2744 kg/m³ as representative of the upper 5 km (Fig. 2).

The details of the soils in the basin are listed in Table 1 and depicted in Figure 2; in all cases we have assumed a Poisson ratio of 0.25 and assigned values of density according to the values suggested by Grant and West, (1965) (their figures 7-1 and 7-7), assuming wet bulk density. In Figure 2, (a) and (b) show the topography of the free surface of the region (water not included) and the topography of the bed-

rock, respectively. The blue line in (a) is the datum level taken as the flat free-surface for the modeling. In between these two surfaces are the layers of soils described above, illustrated by the interfaces in (c), cut along the line AB′ in (a). These are, from bottom to top, the graywacke bedrock (blue), the stiff Brunswick interglacial sediments (light brown), the poorly consolidated Waimea sediments (brown), and the soft Last Glacial sediments (gray). In (d) we illustrate the position of the bedrock topography of the Wellington region model with respect to the 1D model of Robinson (1986).

As pointed out above, the P and S velocities and density profiles of each layer of sediments exhibit gradients. The 3D variability of the seismic-wave velocities and density is shown in Figure 3, for five sites indicated in Figure 2a. The profile "Bay" is on the fault just below the profile AB, where the basin is deepest.

Method

Numerical modeling of earthquakes and seismic-wave propagation in realistic, 3D geological structures to study strong ground motion has become possible thanks to the advent of large, efficient computers. The most commonly used numerical method for that purpose is finite differences (e.g., Olsen, 1994; Graves 1996). In this work we use the finite-differences scheme of Olsen (1994, 2000), with accuracy of fourth order in space and second order in time. A coarse-grained viscoelasticity approach (Day, 1998) is used to calculate anelastic attenuation (Q) in the part of the model containing the sediments (0- to 900-m depth) that is implemented with stress relaxation independently for both P and S waves using a standard linear solid. We assume that Q_s = 0.02 V_s (m/sec) for V_s < 1500 m/sec and Q_s = 0.1 V_s (m/sec) for V_s > 1500 m/sec, and Q_p = 1.5Q_s. This relationship was found to provide the best fit to observed peak velocities for the 1994 Northridge earthquake in the Los Angeles basin (Olsen *et al.*, 2003). A purely elastic scheme is applied to

Table 2
3D Modeling Parameters

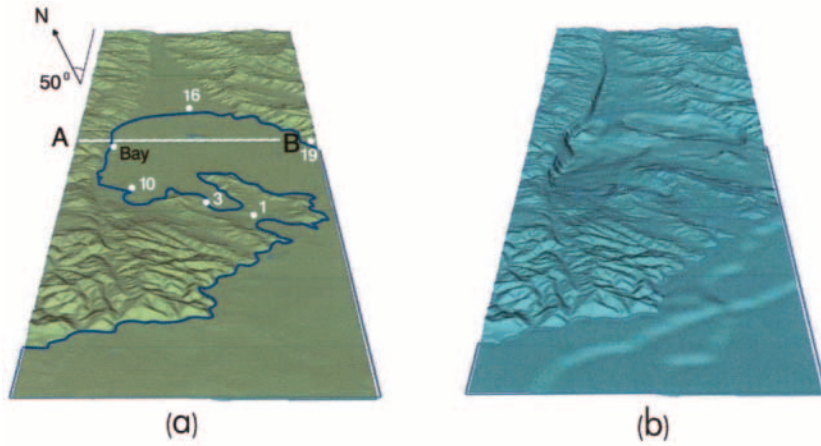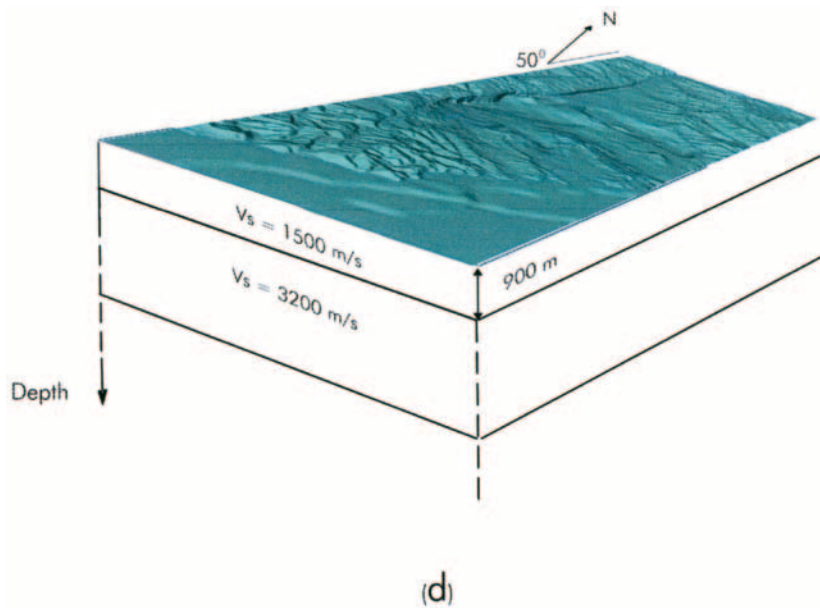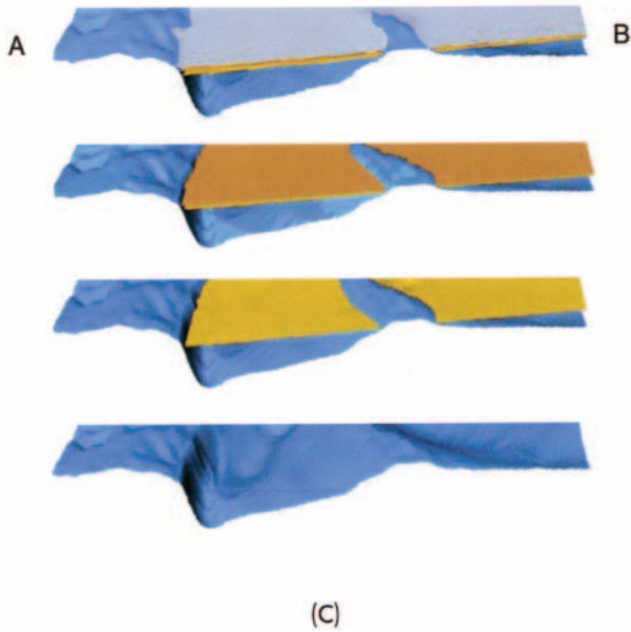|	
Spatial discretization (m)	40
Temporal discretization (sec)	0.0035
Lowest P-wave velocity (km/sec)	0.52
Lowest S-wave velocity (km/sec)	0.3
Lowest density (kg/m³)	2,254
Highest P-wave velocity (km/sec)	5.4
Highest S-wave velocity (km/sec)	3.4
Highest density (kg/m³)	2,744
Number of grid points along 50°	955
Number of grid points along 320°	290
Number of grid points along vertical	240
Hypocentral depth (km)	7.6
Number of timesteps	17,143
Simulation time (sec)	60

Figure 2. (a) The full free-surface digital model, the blue line is the shoreline, (b) bedrock (graywacke) basin interface. The model is 30 km long (north is up) and 10 km wide. The grid spacing is 40 m. (c) A cross section along the line AB′ in (a), crossing the harbour, touching the southern tip of the Somes Island. There are three layers of soils (four interfaces) in between the free-surface and the basin bedrock topographies, depicted by the four plots, described in the text. In (d) we illustrate the position of the bedrock interface with respect to the 1-D model used for hypocenter location (Robinson, 1986).

the bedrock below the sediments, in order to limit computational requirements. The simulation required approximately 2 CPU days on each of 12 processors on an 195 MHz SGI Origin 2000 computer.

The geological model is discretized with a grid spacing equivalent to 5 nodes per minimum shear wavelength of 200 m, which limits the maximum resolved frequency to 1.5 Hz. The full digital model is discretized at 40-m spacing into 66 million grid points. The 3D modeling parameters are listed in Table 2 (see page 2182).

Rupture Scenarios

Two rupture scenarios are considered in this work; the first is with the hypocenter at the southernmost tip of the fault at 7.6-km depth and with the rupture front propagating outward toward the north. The second is with the hypocenter at the northernmost tip of the fault at 7.6-km depth and the rupture front propagating outward toward the south. In both cases the rupture velocity is 90% of the bedrock S-wave velocity. It is worth pointing out recent studies of stress dis-
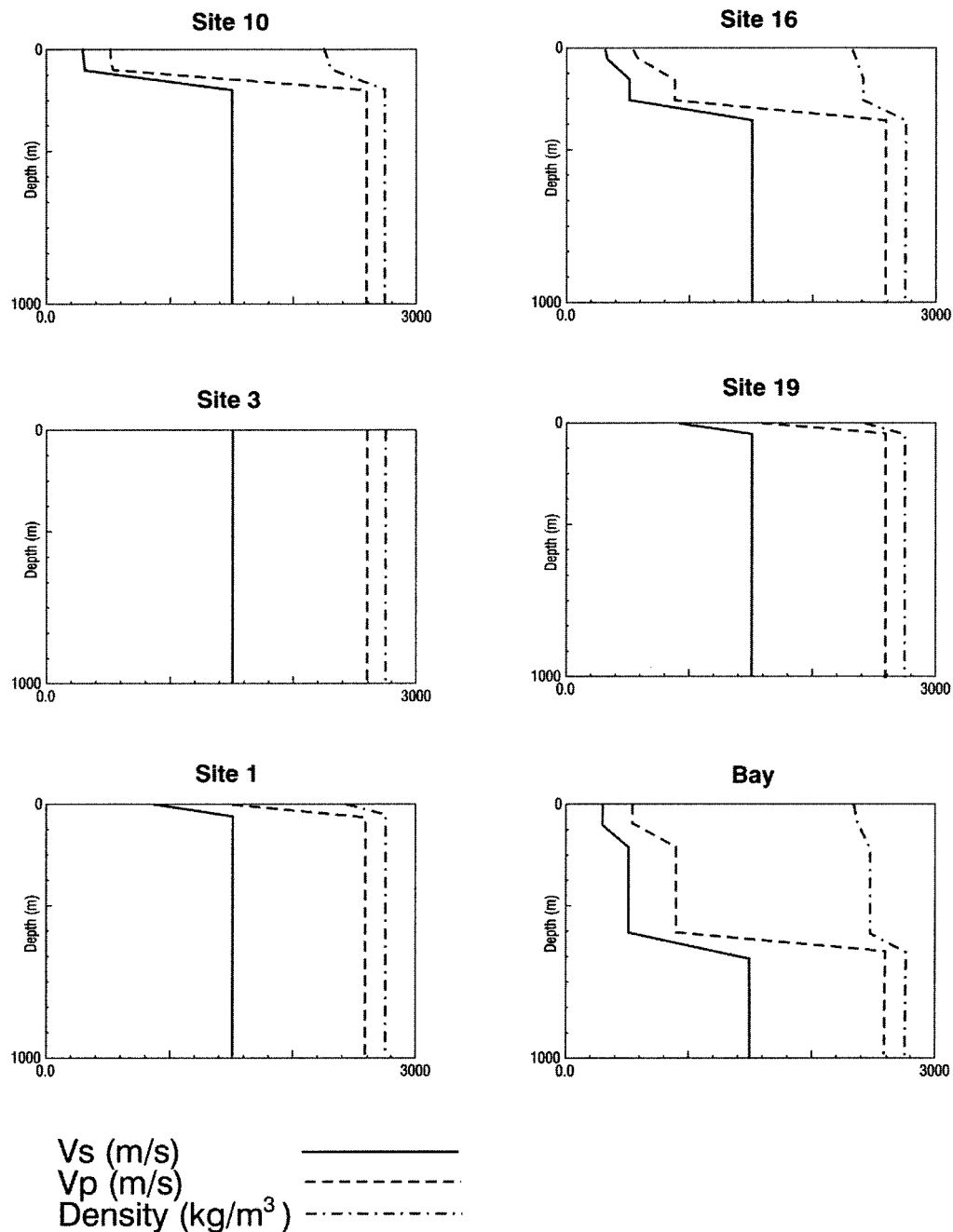

Figure 3.   Seismic wave velocities (S wave: full line, P wave: dashed line) and densities (dot-dashed line) at selected points in the region (see Fig. 2a).
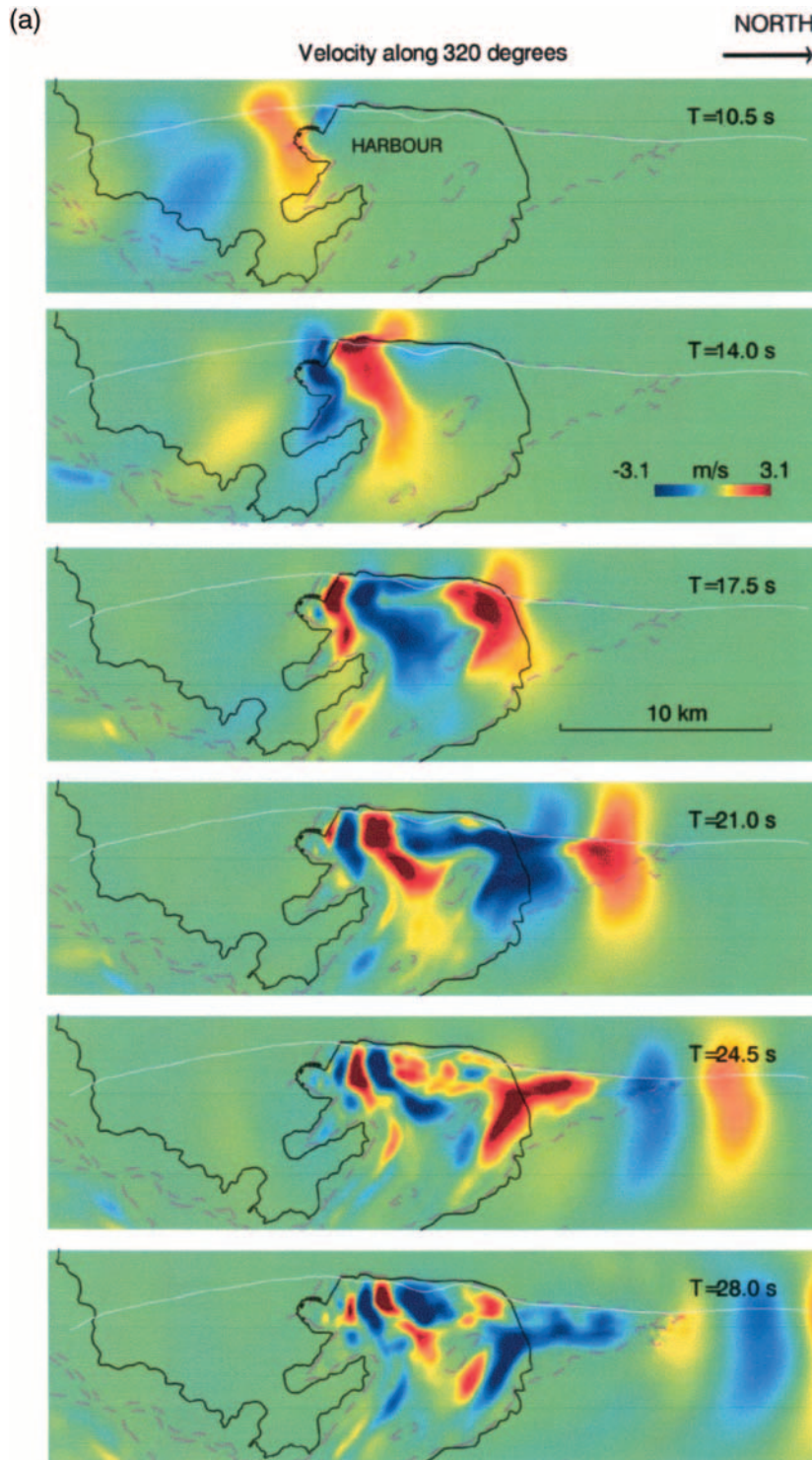
Figure 4. Time snapshots at five selected times *T* of the ground motion in the Wellington region, for the component perpendicular to the fault strike (320° from the true north). The whole region has been rotated 50° clockwise with respect to the true north. (a) South-to-north rupture; (b) north-to-south rupture.

(*continued on next page*)

tributions (Han 2003) that show that the level of stress beneath the Cook Strait section of the fault may be high, favoring a rupture direction from south to north.

The rupture scenarios are kinematically simulated by using a variable slip distribution, as in Olsen (2000), with slip values taken from the kinematic inversion results of Wald and Heaton (1994) for the *M* 7.3, 1992 Landers, California, earthquake. The slip distributions are incorporated on 100 subfaults (5 × 20). The slip rate function is of triangular shape, with a rise time of 2 sec. The source is implemented in the finite-difference grid by adding $-M_{ij}(t)/V$ to $S_{ij}(t)$, where $M_{ij}(t)$ is the *ij*th component of the moment tensor for the earthquake, $V = dx^3$ is the cell volume, and $S_{ij}(t)$ is the *ij*th component of the stress tensor on the fault at time *t*. The
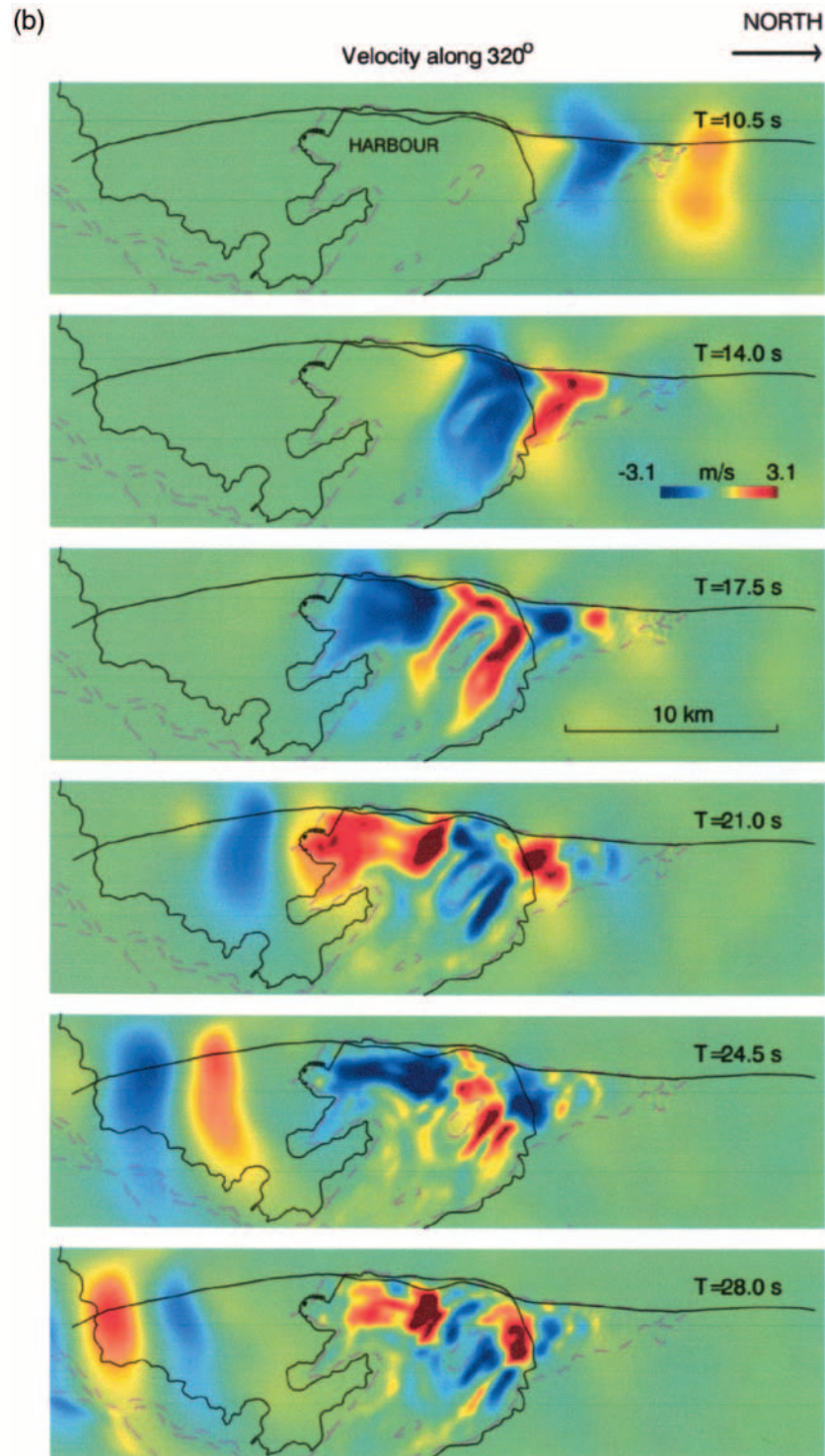
Figure 4. Continued.

synthetic seismograms are low-pass filtered for frequencies less than 1.5 Hz (butterworth filter with 4 poles and 2 passes). In the model, the fault is attached to the bedrock. The average slip chosen here for the Wellington fault is 1.5 m, compared to 1.3 for the *M* 6.7, 1994 Northridge, California, earthquake.

Results and Analysis of Seismic-Wave Propagation

The ground motions, in terms of particle velocity, for both earthquake scenarios are shown in Figure 4 (a) for the rupture south-to-north (S–N) and (b) for the rupture north-to-south (N–S), for time snapshot frames, starting at 10.5 sec
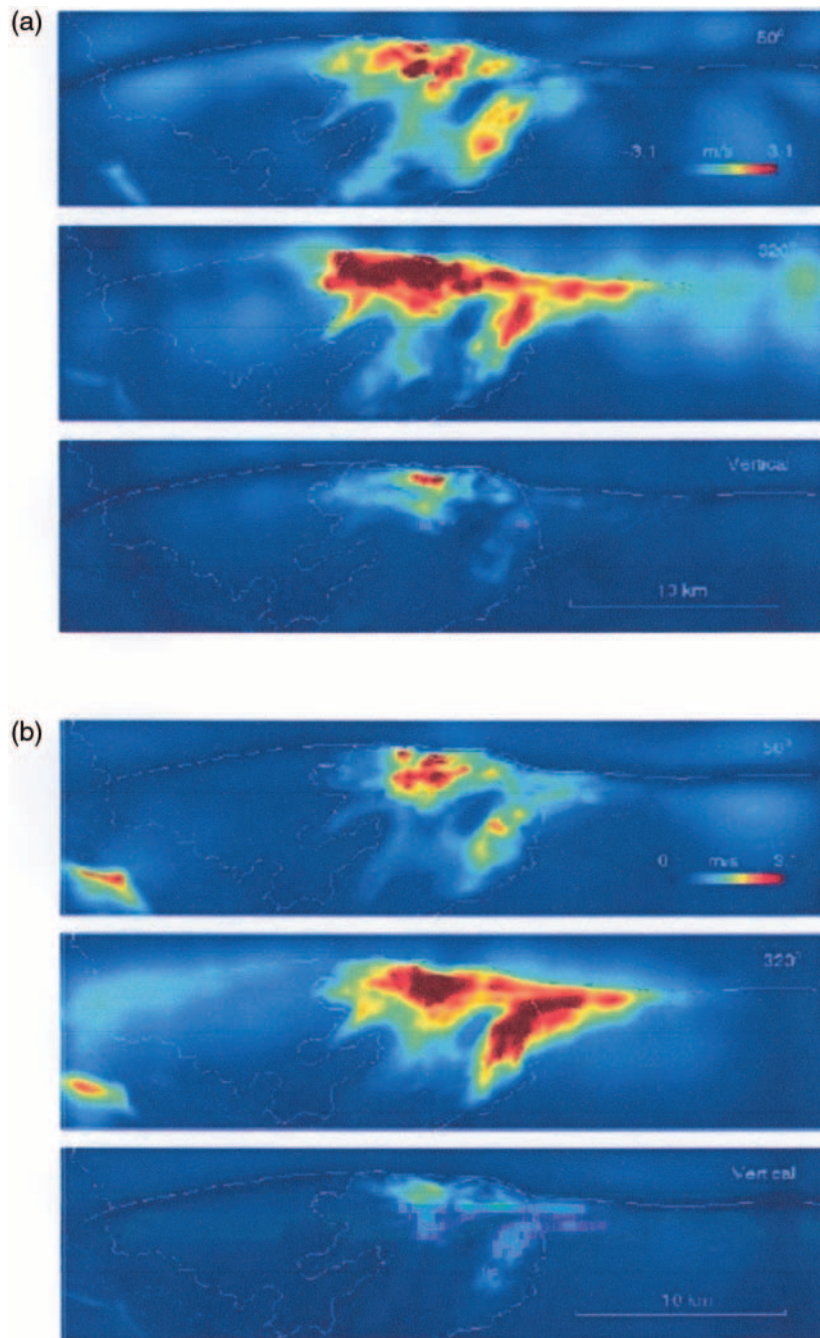
Figure 5. Peak ground velocities in the Wellington region (a) for the south-to-north rupture and (b) for the north-to-south rupture. The panels correspond to the motion parallel (top) and perpendicular (middle) to the fault, and vertical motion (bottom).

after the rupture initiation and at increments of 3.5 sec. For display purposes, we have rotated the plan view of the region (the white line represents the fault) 50° clockwise from north, using the directions 50° and 320°, clockwise from north, to describe the horizontal components of the ground motion. In Figure 4 the motion in both cases corresponds to the component perpendicular to the strike of the fault (i.e., ~320° from true north).

The snapshots show that the seismic response of the region depends on the rupture direction, in particular for the large wavelengths (corresponding to periods > 1 sec). For

small wavelengths (periods < 1 sec) the ground motion seems to be confined to the Wellington harbor only, where the duration of the seismograms is the largest, for both rupture directions.

In the case of a south–north rupture there are two dominant effects. The first is resonance, of periods between 2.4 and 3.3 sec, toward the northern part of Wellington harbor, close to the fault, where the depth of the sediments is greatest (580 m) in the model. The second is focusing of the incident wave on the Lower Hutt area due to the shape of the bedrock (like a prolated ridge) that emerges in the Wellington harbor

as Somes Island. We note that the triangular shape of the Lower Hutt Valley, with the bedrock pinching out toward the north, may also impose focusing on the horizontal components of the wavefield, but quantifying this effect properly would require further modeling. In the case of the north–south rupture, large amplitudes are also observed in the harbor for the same periods as for the south–north rupture, and deflection of the seismic energy by the Somes Island, as opposite to the focusing in the south–north case. Since this is a rather descriptive characterization of the wave propagation, the reader is encouraged to observe the animations in the supplement (Ⓔ available in the electronic edition of BSSA.).

Considering the three components of motion, the amplitudes of both the component parallel to the fault strike (50°) and the vertical component are, in general, about 10% larger for the south–north rupture than for the north–south, while the component perpendicular to the fault strike (320°) is about the same for both rupture directions. This can be seen in Figure 5, where the spatial distributions of maximum amplitudes for the three components are shown (a) for the south–north rupture and (b) for the north–south rupture. We have calculated the absolute peak values of the motion at every grid point on the surface of the model. From these results we conclude that, in general, the maximum amplitudes of ground motion in the Wellington region are about the same for both rupture directions, but their spatial distribution depends on the rupture direction. The seismic radiation from the fault is basically the same for both rupture directions, except for slight differences imposed, in our case, by the assumed fault segmentation and by the slip distribution on the fault plane.

The peak ground motions, in terms of particle velocity, rendered by the modeling are quite large, up to about 3 m/sec. The largest peak velocities occur mostly in the harbor and most likely are due to the thicker soft sediments there than elsewhere in the region. To our knowledge, one of the largest reported peak ground velocities in the near field (within 5 km of the surface rupture) is for the Rinaldi receiving station during the 1994 M_w 6.7 Northridge earthquake of 1.77 m/sec, corresponding to 0.85g acceleration (Hall *et al.*, 1995).

Next, we incorporate variable slip rise time for the rupture of each subfault for both north–south and south–north earthquake scenarios. We use the rise time varying linearly between 0.5 sec and 3 sec for slip between 0.5 and 2.5 m, as depicted in Figure 6. Results show that the radiation patterns are, basically, the same as those without the variable slip rise time, but the maximum particle velocity amplitude reduces by about 25%, to 2.6 m/sec. This is shown in Figure 7 for the south–north rupture.

Although we have incorporated material attenuation in our modeling via quality factors that are linearly related to the shear-wave velocity, we believe that smaller, more realistic amplitudes can be obtained by incorporating the attenuation due to the nonlinearity of the softer, superficial,
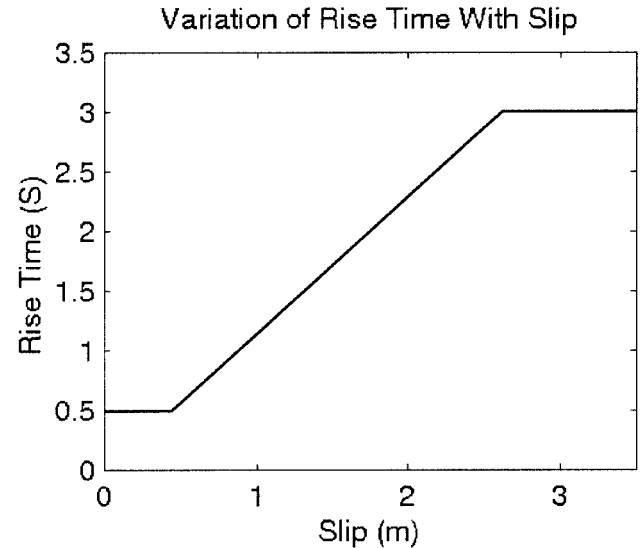

Figure 6.   Rise time versus slip, for the simulations with variable rise time.

soils of Table 1. This is outside the scope of the present work.

Amplification Factors

Spectral ratios with respect to a reference station on rock using observed teleseismic earthquakes are, to some extent, measures of the local site effects. This type of measure cannot be applied here because the basic assumptions for teleseismic incidence do not hold in the near field. Instead, we compute spectral ratios with respect to the corresponding 1D models for each of the rupture scenarios, that is, we compare the ground motions produced by the earthquake in media with and without the basin structure.

In what follows, we use the standard technique of spectral ratios between corresponding 3D/1D reference components, using Fourier spectra.

Referring to Figure 8, we have selected a total of 31 sites over the Wellington Metropolitan Region, 22 represented by dots and labeled from s1 to s22, and 9 represented with diamonds, not labeled, distributed across and along the Lower Hutt Valley. Of the 22 labeled sites we have chosen 18 to calculate spectral ratios. The group of sites S1 to S9 is called "Wel," and the group S14-S22 "LH." Most of these sites are on, or close to, the sites of the strong ground motion network of New Zealand. We have taken 30-sec time windows to calculate Fourier spectra, each smoothed with a five-point interpolation.

The spectral ratios for the south–north rupture are shown in Figure 9, top for LH, bottom for Wel. The thick gray line in the top panel corresponds to the average of the spectral ratios of 12 sites on the sediments, namely S15, S16, and S17 plus the nine nonlabeled stations. The thin gray line in Wel is site S10, which sits on very soft (reclaimed) soils. The full lines are the individual spectral ratios of sites s14,
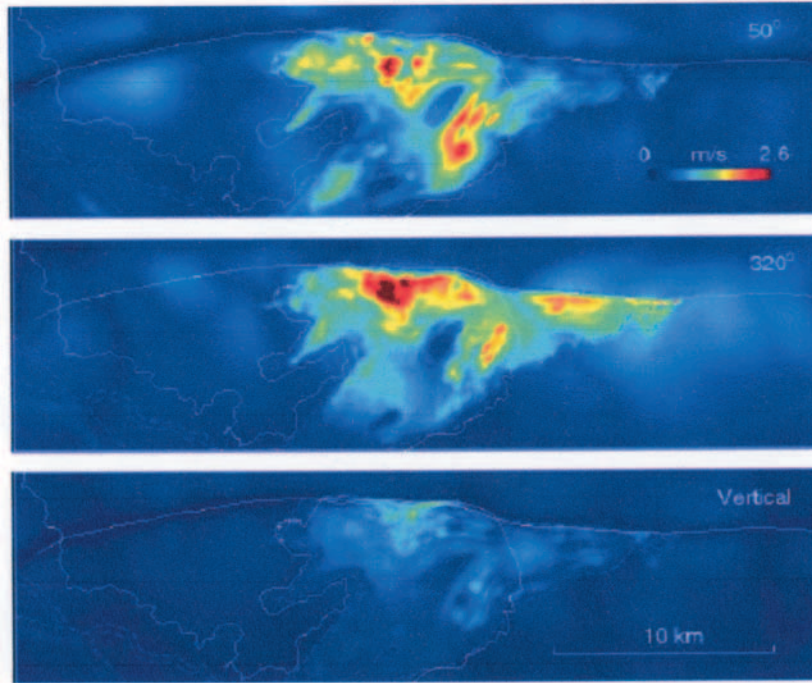
Figure 7. The ground motion for the south-to-north rupture using variable slip rise time (VSRT) for the ruptures at each subfault. Top, middle, and bottom panels are defined as in Figure 5. Note that the maximum amplitude is smaller than that without VSRT, in Figure 5.
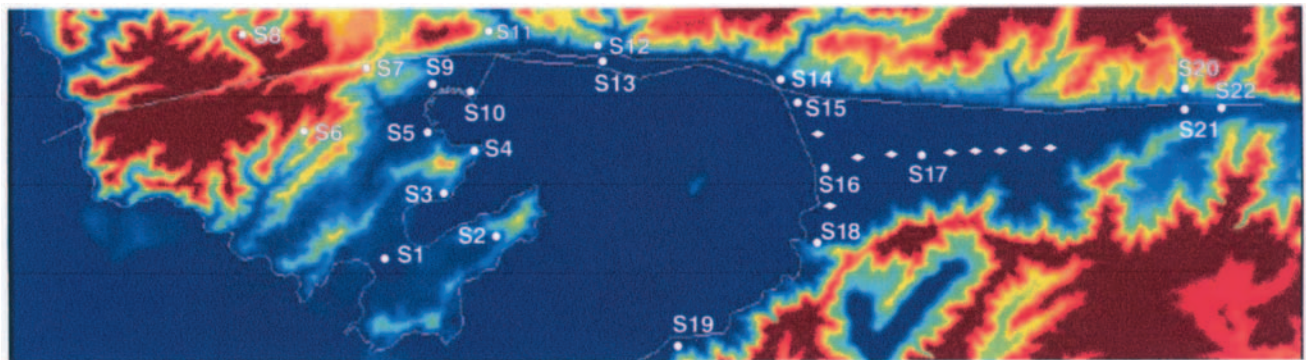

Figure 8. Selected sites in the Wellington Region used to calculate site effects. Colors denote free-surface topography (blue is sea level), and the white line the shore of the harbor, along with the fault.

s18, s19, s20, s21, and s22 in LH, and s1, s2, s3, s4, s5, s7 and s9 in Wel. In general, these full lines correspond to sites on or nearby rock.

The peak of the average spectral ratios between 0.5 and 1.2 Hz determines that the maximum amplification in the region, a factor of 5, occurs on the sediments of the Lower Hutt Valley, on the 320° component. A less prominent peak also occurs for the other components, between 0.5 and 1.2 Hz, yielding amplification factors of up to 3. The ratios for the other sites in Lower Hutt seldom exceed a factor of 2, and on the 320° component the ratios show tendency to fall off below 1, suggesting deamplification. In Wellington the responses are, basically, flat around 1, suggesting no amplification. The exception is site s10, whose response is similar to that of the Lower Hutt sediments.

The spectral ratios for the north–south rupture are shown in Figure 10, arranged in the same way as those in Figure 9. A peak between 0.5 and 1.0 Hz, centered around 0.7 Hz, appears with amplitudes up to 3 on each of the horizontal components. The responses of the other sites in the Lower Hutt Valley show similar variability as those for the south–north rupture, while the responses in Wellington show more variability than those for the south–north rupture, individually exceeding factors of 4. The response of site S10, again, has similar characteristics to that of the sediments in Lower Hutt, peaking between 0.5 and 0.7 Hz, with maximum amplitude 4 on the 320° component.

It must be noted that in the Lower Hutt Valley amplification factors on the horizontal motion of over 10 at frequencies between 0.5 and 8 Hz have been reported by Taber
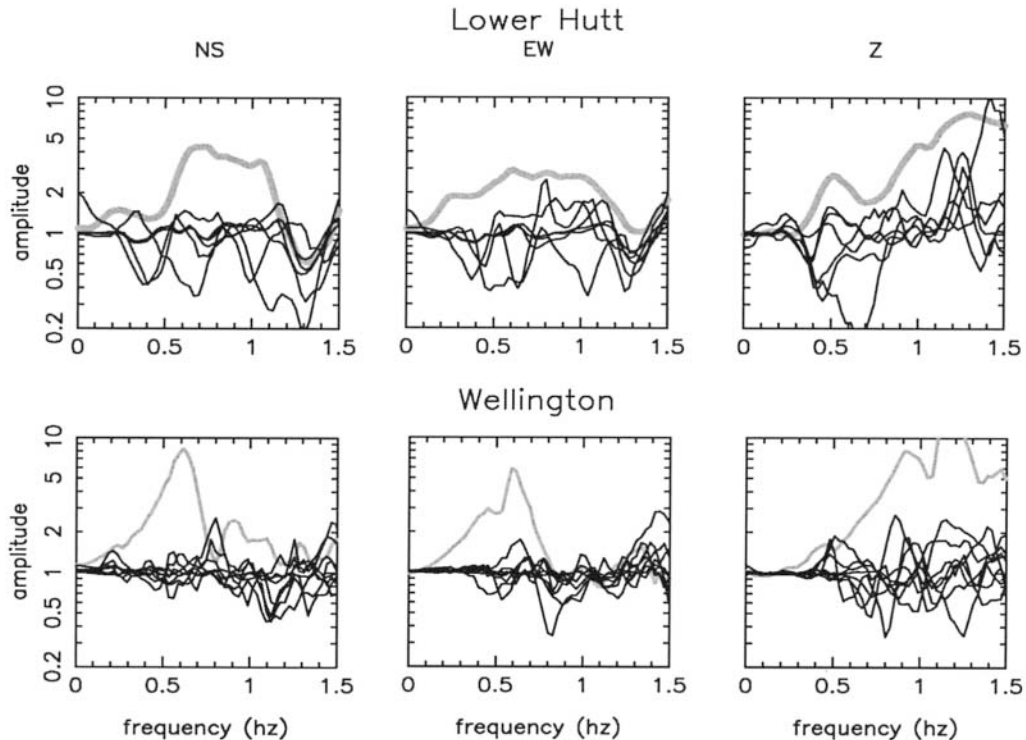
Figure 9.   3D/1D spectral ratios for the south-to-north rupture scenario, top for the Lower Hutt valley, bottom for Wellington City. The components NS (320°), EW (50°), and Z correspond to perpendicular to the strike of the Wellington Fault, parallel to the strike, and vertical components, respectively. In the top figure, the thick gray line denotes the average of the ratios at sites S15, S16, and S17 plus the nine unlabelled stations, on thick soft sediments in the Lower Hutt valley. In the bottom figure, the thin gray line corresponds to the ratio at site S10, on soft, reclaimed land. In both, the thin full lines are the ratios at the other sites, plotted individually, mostly on stiffer soils or rock.

and Smith (1992) using observed weak motion, and by Sritharan and McVerry (1992), using observed strong ground motion. In particular, their amplification factors in the range 0.5 to 1.5 Hz are up to 7 for the weak motion and up to about 9 for the strong motion. We must point out that in the case of Taber and Smith (1992), 0.5 Hz is the lower limit of the 1-Hz response seismometers used in their experiments.

Adams *et al.* (2003) also produced spectral ratios for up to 5 Hz due to, basically, weak motion, at eight stations distributed along a line perpendicular to the Wellington fault, in the Hutt Valley. The location of these stations is, roughly, about 1 km north of our site S15, along the fault. Their reference station on rock is close to our S18 site. Although the peak values of Adams *et al.* (2003) spectral ratios for the horizontal components occur mostly above 1.75 Hz, their behavior with frequency and amplitude (about factor of 5) are comparable with our results within 0.5–1.5 Hz (figure 11 of their article). Adams *et al.* (2003) associate their peak values to the so called basin-edge effect.

We believe that the peak between 0.5 and 1.2 Hz, centered around 0.65 Hz, on the 320° component in the Hutt Valley is not due to fault-rupture propagation effects, such as directivity, but is related to the effects of the basin. To

demonstrate this, we have calculated the Fourier spectra at sites S7, S11, S12, S14, S20, and S22 (Fig. 8) along the fault, in the absence of the basin (1D), for the two rupture scenarios. These spectra, for the three components and at each site, are shown in Figure 11, in which the black line corresponds to the south–north rupture and the gray line to the north–south rupture. The spectra show that the directivity effect is about the same for both rupture directions and that the level of the spectra increases in the direction of rupture, peaking between 0.2 and 0.4 Hz at all the selected sites for fault-normal motions.

Off the fault, the effect of fault-rupture directivity decreases with distance from the fault, as shown in Figure 12, where we have computed the Fourier spectra at sites S14, S15, S16, S18, and S19 (Fig. 8) in the Lower Hutt Valley for 1D models of south–north (black line) and north–south ruptures (gray line). The level of Fourier spectra at S19, the site farthest from the fault, is about five times smaller than at S14, the closest site. By comparing these Fourier spectra with their corresponding 3D spectra at the same sites (Fig. 13, black and gray lines for the south–north and north–south, respectively) we notice, first, that the levels of the 3D Fourier spectra are larger with larger distance off the fault, within a
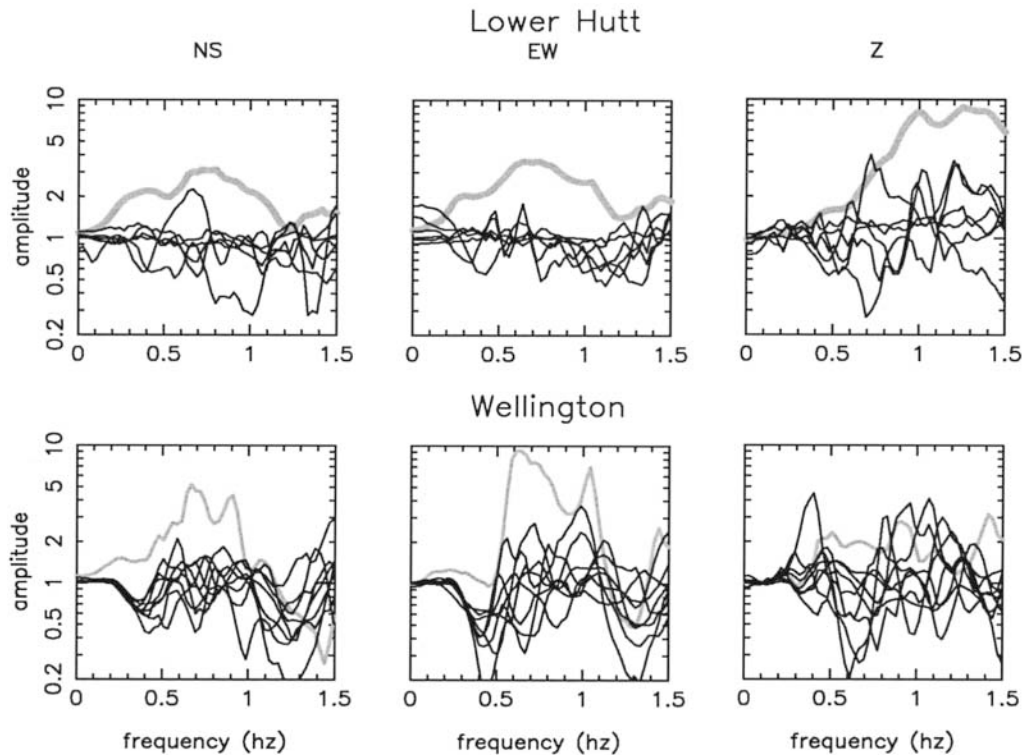
Figure 10.   3D/1D spectral ratios for the north-to-south rupture scenario. Definitions are the same as in Figure 9. Note that the peak between 0.5 Hz and 1 Hz is broader than for the south-to-north rupture, implying the effect of focusing in the latter.

narrow frequency band between 0.4 and 0.7 Hz, peaking at S16, and decreasing at S18. At S19 the 3D spectral level is smaller than its corresponding 1D Fourier spectra. This behavior is similar for both rupture directions.

From those results, it is clear that the peak amplification factor between 0.5 and 1.2 Hz determined by spectral ratios in the Lower Hutt Valley is due to site effects, most likely related to its fundamental response. Let us emphasize the effect of the basin by low-pass filtering the seismograms of the south–north rupture at 0.5 Hz. These are shown in Figure 14, for 36 sites along the dashed line of the model at the top of the figure. Resonance appears at 12 km, close to the south shore of the harbor, and reaches maximum amplitude, of 109 cm/sec on the 320° component (perpendicular to the fault), at 17 km, near the center of the harbor. It is clear from the figure that the waves due to resonance in the harbor contribute strongly to ground shaking, as far as about 25 km, toward the Hutt Valley.

Conclusions

The ground motion in the Greater Wellington Region, New Zealand, upon the impact of *M* 6.7 earthquakes due to ruptures of the Wellington fault has been numerically modeled for frequencies up to 1.5 Hz, and for two earthquake scenarios corresponding to ruptures in the south–north and north–south directions. These ruptures are kinematically

modeled by incorporating slip distributions on 100 subfaults (5 × 20) distributed regularly over the total fault area and assuming variable slip rise time for each. The rupture front velocity is taken as equal to 90% of the bedrock *S*-wave velocity.

The modeling reveals that the character of the 3D seismic-wave propagation in the region varies with rupture direction, exhibiting resonance at periods about 3 sec (0.34 Hz) and focusing upon the Lower Hutt Valley for the south–north scenario and deflection of seismic energy (as opposed to focusing) for the north–south scenario. A common feature of wave propagation is the long-lasting reverberations of the higher frequency waves ($\geq$1 Hz) in the harbor, after the ruptures have stopped. Although both rupture directions render comparable seismic-wave amplitudes, the spatial distributions of peak ground velocity are slightly different. The maximum peak values (2.6 m/sec) appear distributed over a more extended area of the Lower Hutt Valley for the north–south than for the south–north scenario. On the other hand, the maximum peak values are rather distributed over a narrow area along the fault for the south–north rupture.

In general, the characteristics of the spectral ratios in the region are similar for both ruptures, and the major feature of the site response rendered by our modeling in the frequency range up to 1.5 Hz is a maximum amplification factor of about 4 in the horizontal ground motion of the Lower
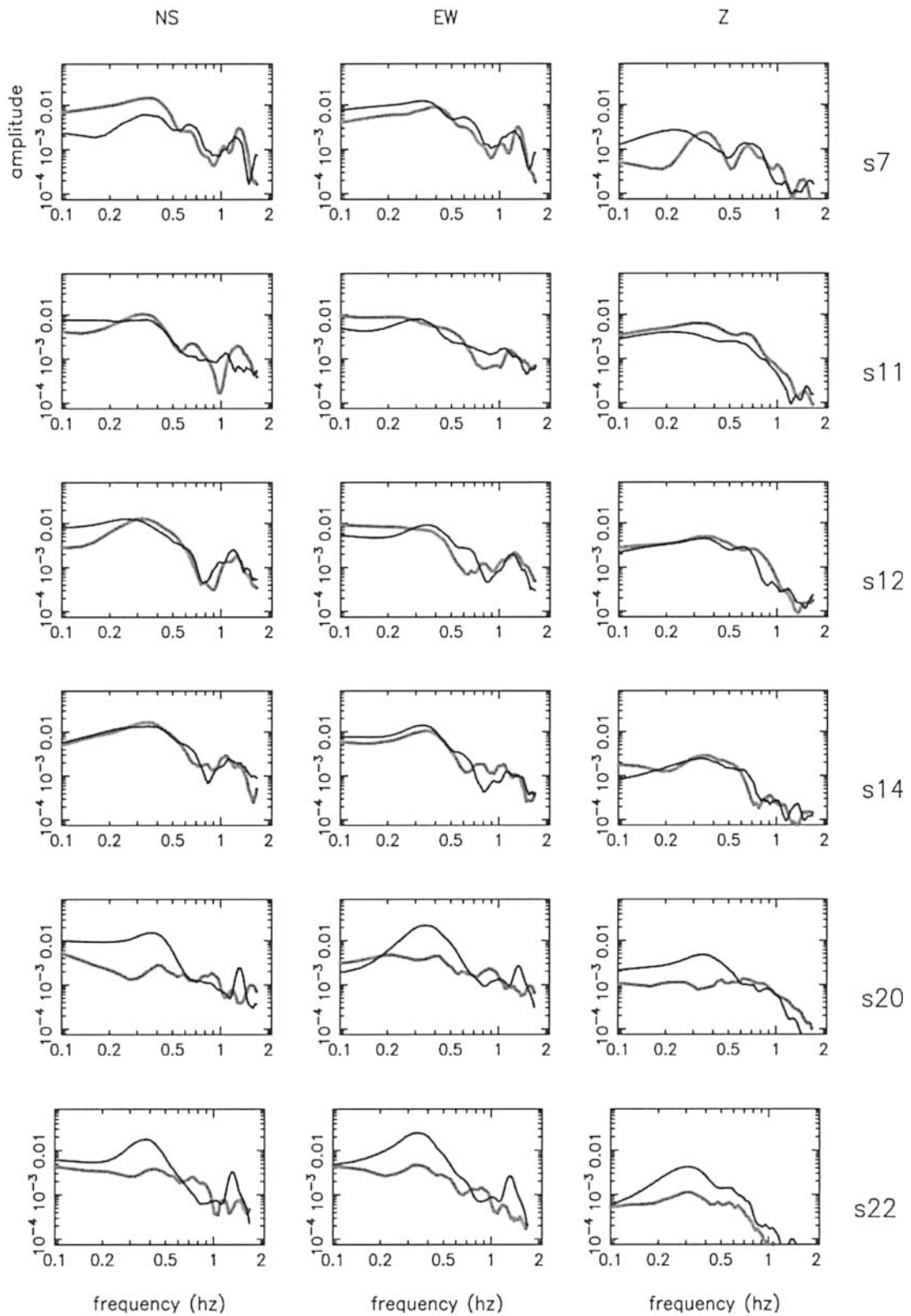
Figure 11.   Spectra at sites S7, S11, S12, S14, S20, and S22 of Figure 8, for the 1D south-to-north rupture (black line) and for the 1D north-to-south rupture (gray line). NS (320°), EW (50°), and Z denote components perpendicular and parallel to the fault strike, and vertical, respectively.
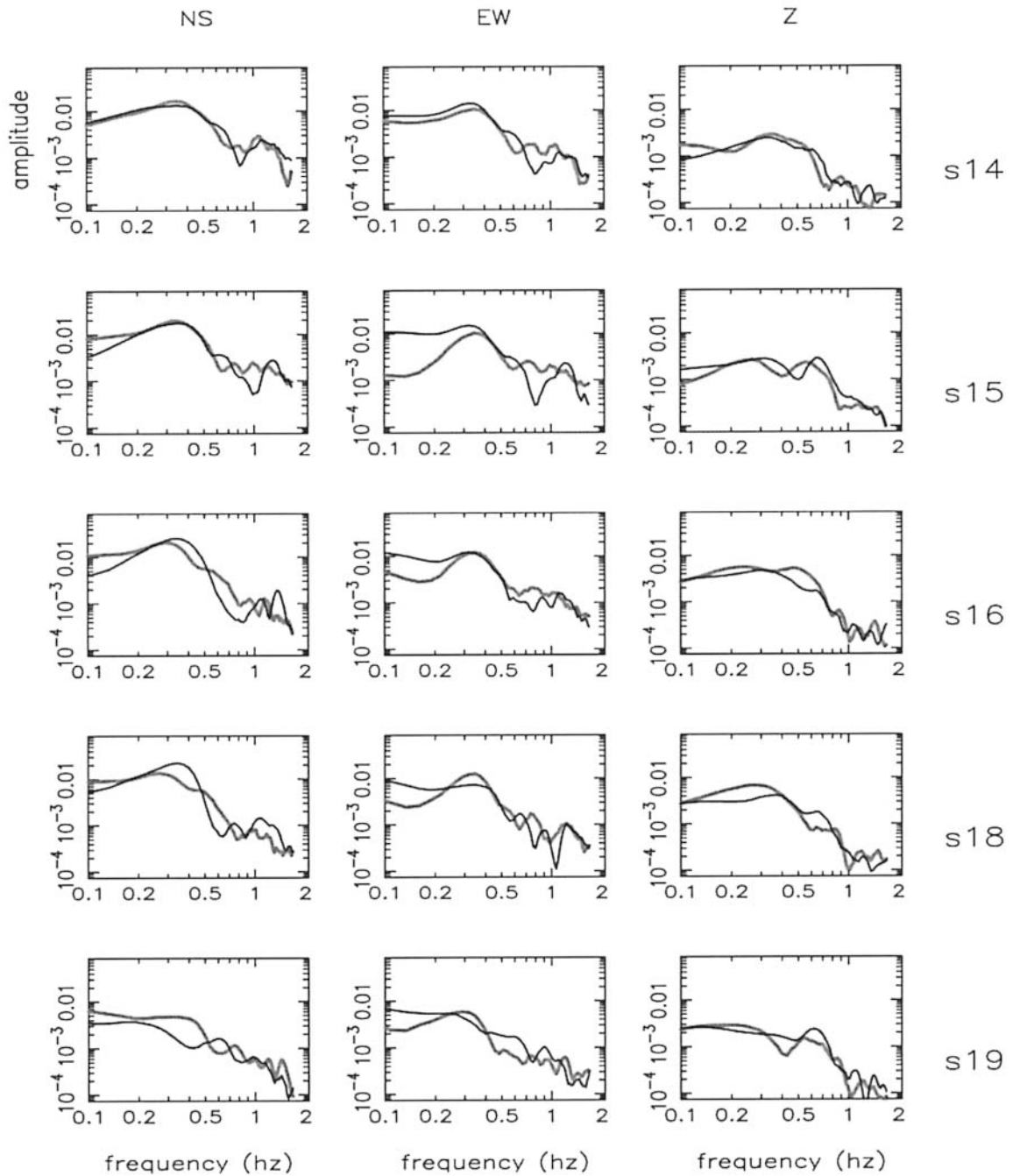
Figure 12.   Spectra at sites S14, S15, S16, S18, and S19 of Figure 8 for the 1D south-to-north rupture (black line) and for the 1D north-to-south rupture (gray line). Other definitions are the same as for Figure 11.

Hutt Valley, between 0.5 and 1.2 Hz, centered at about 0.65 Hz. The peak spectral ratio conveying this amplification factor appears slightly less broad for the south–north rupture, suggesting the effect of focusing.

Considering the source radiation only (1D), the Fourier spectra for stations distributed both along the fault and off the fault in the Lower Hutt Valley peak between 0.2 and 0.4 Hz, in all cases. However, when the 3D structure is incorporated, Fourier spectra in the Lower Hutt Valley peak between 0.4 and 0.7 Hz, suggesting, in turn, that such amplification factors are not due to fault-rupture propagation but to site effects, most likely related to the natural response of the whole basin.

Regarding future studies following up on the work reported in this article, we have considered several cases. As mentioned above, the expected magnitude of a characteristic earthquake on the Wellington–Hutt Valley segment is between *M* 7.2 and 7.4. We believe that an immediate task is
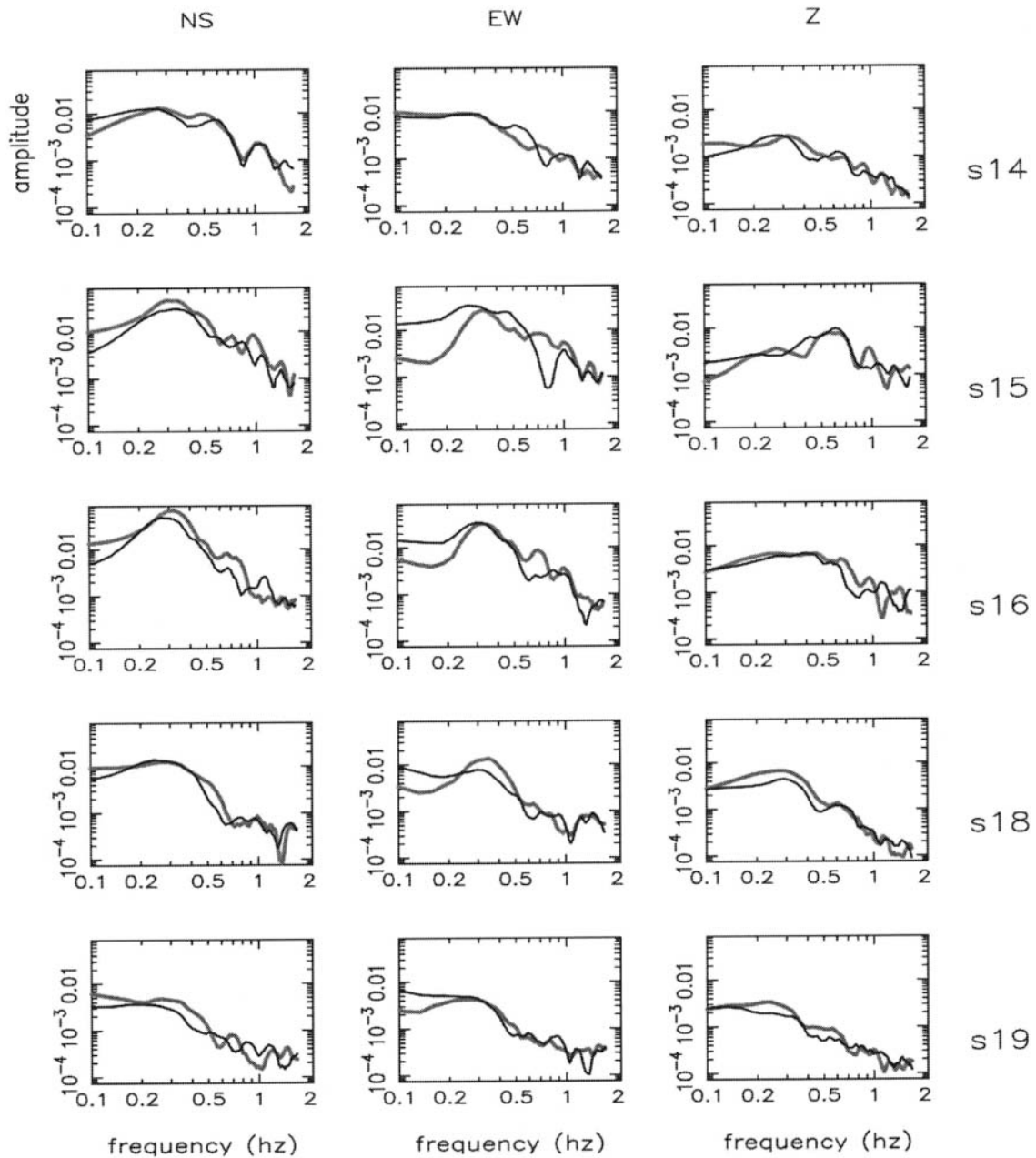
Figure 13.   Spectra at sites S14, S15, S16, S18, and S19 of Figure 8 for the 3D model of rupture for south-to-north (black line) and for the north-to-south (gray line). These spectra are to be compared with the corresponding 1D spectra of Figure 12.

to compute strong ground motion in the Wellington Metropolitan Area for several characteristic earthquake scenarios, considering ruptures of the full length of the segment, 75 km, and by assigning a fault width of 20 km (Robinson, 1986).

The 3D digital model used in this work has been built from all presently available data on the stratigraphy of the region. We are aware that the 3D crustal model should be improved, in particular if we want to increase our frequency range. It is of crucial importance to know, accurately, the topography of the bedrock close to the fault-bounded edge

of the basin, since strong resonances seem to originate in this area.
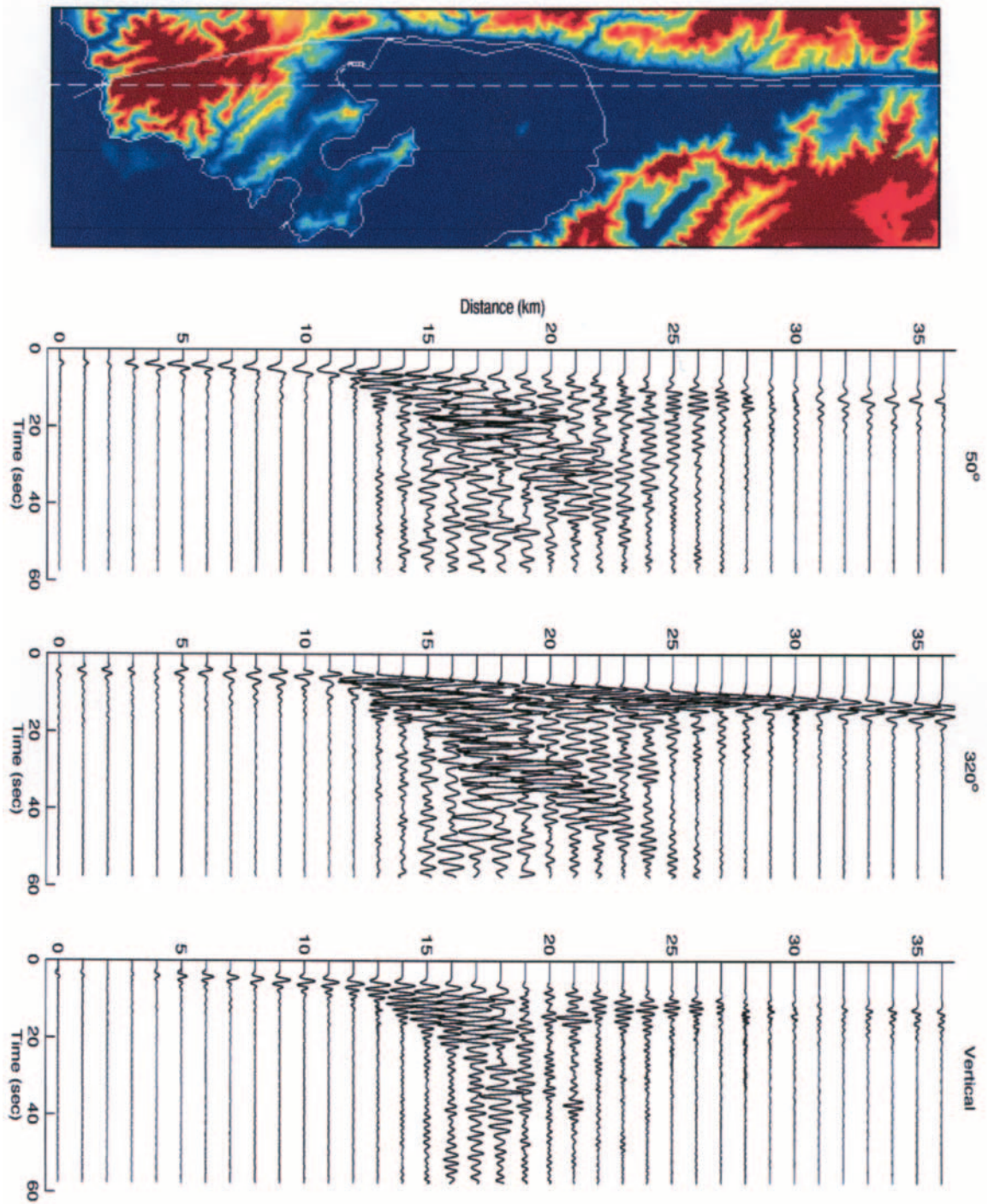
Acknowledgments

Figure 14.   Time-domain seismograms corresponding to 0.5-Hz ground motion at 36 stations regularly distributed along the dashed line of the model at the top, for the south-to-north rupture.

ity of our manuscript. The simulations were carried out on the SGI Origin 2000 at the University of California at Santa Barbara, California. The model parameters can be obtained by contacting the authors at R.Benites@gns.cri.nz, and kbolsen@sciences.sdsu.edu.

(Ⓔ The ground-motion simulations are available in the electronic edition of BSSA.)

References

Adams, B. M. (2000). Basin-edge effects from SH-wave modeling with reference to the Lower Hutt Valley, New Zealand, *Ph.D. Thesis*, University of Canterbury, Christchurch, New Zealand, 270 pp.

Adams, B. M., N. M. Osborne, and J. J. Taber (2003). The basin-edge

effects from weak ground motions across the fault-bounded edge of the Lower Hutt Valley, New Zealand, *Bull. Seism. Soc. Am.* **93,** 2703–2716.

Berryman, K. R. (1990). Late Quaternary movement of the Wellington Fault in the Upper Hutt area, New Zealand, *New Zealand J. Geol. Geophys.* **33,** 257–270.

Bouchon, M. (1981). A simple method to calculate Green's functions for elastic layered media, *Bull. Seism. Soc. Am.* **71,** 959–971.

Day, S. M. (1998). Efficient simulation of constant Q using coarse-grained memory variables, *Bull. Seism. Soc. Am.* **88,** 1051–1062.

Dellow, G. D., S. A. L. Read, J. G. Begg, R. J. Van Dissen, and N. D. Perrin (1992). Distribution of geological materials in Lower Hutt and Porirua, New Zealand: a component of a ground shaking hazard assessment, *Bull. New Zealand Natl. Soc. Earthquake Eng.* **25,** no. 4, 332–344.

Grant, F. S., and G. F. West (1965). Interpretation theory in applied geophysics, in *International Series in the Earth Sciences*, R. R. Shrock (Consulting Editor), McGraw-Hill, New York, 583 pp.

Graves, R. W. (1996). Simulating seismic wave propagation in 3D elastic media using staggered-grid finite differences, *Bull. Seism. Soc. Am.* **86,** 1091–1106.

Hall, J. F., T. H. Heaton, M. W. Halling, and D. J. Wald (1995). Near-source ground motion and its effects on flexible buildings, *Earthquake Spectra* **11,** 569–605.

Han, Z. (2003). Possible reduction of earthquake hazard on the Wellington Fault, New Zealand, after the nearby 1855, M 8.2 Wairarapa earthquake and implications for interpreting paleoearthquake intervals, *Ann. Geophys.*, **46,** 1141–1154.

Langridge, R. M., K. R. Berryman, and R. J. Van Dissen (2005). Defining the geometric segmentation and Holocene slip rate of the Wellington Fault, New Zealand: the Pahiatua section, *New Zealand J. Geol. Geophys.* **48,** 591–607.

Olsen, K. B. (1994). Simulation of three-dimensional wave propagation in the Salt Lake Basin, *Ph.D. Thesis*, University of Utah, Salt Lake City, 157 pp.

Olsen, K. B. (2000). Site amplification in the Los Angeles Basin from 3D modeling of strong ground motion, *Bull. Seism. Soc. Am.* **90,** s77–s94.

Olsen, K. B., S. M. Day, and C. R. Bradley (2003). Estimation of Q for long-period (>2 s) waves in the Los Angeles Basin, *Bull. Seis. Soc. Am.* **93,** 627–638.

Robinson, R. (1986). Seismicity, structure, and tectonics of the Wellington region, New Zealand, *Geophys. J. R. Astron. Soc.* **87,** 379–409.

Sritharan, S., and G. H. McVerry (1992). Microzone effects in the Hutt Valley in records from a Strong-Motion Accelerograph array, *Bull. New Zealand Natl. Soc. Earthquake Eng.* **25,** no. 4, 246–264.

Taber, J. J., and E. G. C. Smith (1992). Frequency dependent amplification of weak ground motions in Porirua and Lower Hutt, New Zealand, *Bull. New Zealand Natl. Soc. Earthquake Eng.* **25,** no. (4), 303–331.

Van Dissen, R. J., K. R. Berryman, J. R. Pettinga, and N. L. Hill (1992). Paleoseismicity of the Wellington–Hutt Valley segment of the Wellington Fault, *New Zealand J. Geol. Geophys.* **35,** 165–176.

Wald, D. J., and T. H. Heaton (1994). Spatial and temporal distribution of slip for the 28 June 1998 Landers, California, earthquake, *Bull. Seism. Soc. Am.* **84,** 668–691.

Institute of Geological and Nuclear Sciences
Gracefield Research Centre
P.O. Box 30-368
Lower Hutt, New Zealand
  (R.B.)

Department of Geological Sciences
San Diego State University
San Diego California 92182-1020
  (K.B.O.)